Brief communication

Corrosion fatigue behavior of nanoparticle modified iron processed by electron powder bed fusion

Check for updates

Steffen Wackenrohr [1] ✉, Christof Johannes Jaime Torrent [2], Sebastian Herbst[1], Florian Nürnberger[1], Philipp Krooss [2], Johanna-Maria Frenck[2], Christoph Ebbert[3], Markus Voigt[3], Guido Grundmeier[3], Thomas Niendorf[2] & Hans Jürgen Maier [1]

Due to its excellent biocompatibility, pure iron is a very promising implant material, but often features corrosion rates that are too low. Using additive manufacturing and modified powders the microstructure and, thus, the material properties, e.g., the corrosion properties, can be tailored for specific applications. Within the scope of this study, pure iron powder was modified with different amounts of CeO_2 or Fe_2O_3 nanoparticles and subsequently processed by Electron Beam Powder Bed Fusion (PBF-EB/M). The corrosion-fatigue behavior of CeO_2 and Fe_2O_3 modified iron was investigated using rotation bending tests under the influence of simulated body fluid (m-SBF). While the modification using Fe_2O_3 showed reduced fatigue and corrosion-fatigue strengths, it could be demonstrated that the modification with CeO_2 is characterized by improved fatigue properties. The superior fatigue properties in air are attributed to the positive impact of dispersion strengthening. Additionally, an increased degradation rate compared to pure iron could be observed, eventually promoting an earlier failure of the specimens in the corrosion fatigue tests.

In the biomedical sector additive manufacturing (AM) has become increasingly important in recent years. This is due to the high design freedom and, eventually, the possibilities to specifically adapt the implant to the patient and location of application[1]. In addition to other processes in AM, Electron Beam Powder Bed Fusion (PBF-EB/M) has become widely established in the past few years[2]. Due to a high probability of presence of process-related defects, the fatigue behavior of additively manufactured components is a key aspect, as defects have a huge effect on the fatigue behavior of any component[3,4]. However, the fatigue strength of AM materials can be equivalent, or even superior, to that of conventionally processed material when an adequate microstructure is established and the process parameters are adjusted to minimize the fraction of or even avoid internal defects[5]. It was further shown for PBF-EB/M processed pure iron that based on an appropriate microstructure design, i.e., a microstructure being characterized by low angle grain boundaries (LAGB), the fatigue strengths is superior to conventionally processed materials[6].

Materials based on magnesium or zinc have been established as common biodegradable implant materials within the last few years[7,8]. However, for applications where the implants are subjected to high mechanical loads, materials with superior mechanical properties, such as iron, are required[9]. Here, a possible application are stents, as iron-based materials are characterized by higher strengths and Young's moduli compared to magnesium-based alloys[10]. Another feasible application is the development of degradable intramedullary nails to avoid explant surgery. At present, intramedullary nails are often based on titanium materials[11]. However, the challenge is to increase the corrosion and the degradation, respectively, as they are often too low for in vivo applications[12,13]. The corrosion rate of as-cast pure iron is approx. 0.008 mm/year[9]. Thus, the main challenge for the application of pure iron as a biodegradable implant material is to increase the degradation through the manufacturing process and/or the related microstructure modification. One possibility here is microalloying. Various studies have shown that alloying with Mn significantly increases the corrosion rates compared to pure iron. Depending on further post-processing, the corrosion rate in Hank's solution can be in between 0.12 to 0.29 mm/year[9,14]. Other elements such as Co, W, C and S also led to an increase in corrosion rates in Hank's solution between 0.142 to 0.187 mm/year[15]. These corrosion

¹Institut für Werkstoffkunde (Materials Science), Leibniz Universität Hannover, An der Universität 2, 30823 Garbsen, Germany. ²Institut für Werkstofftechnik (Materials Engineering), Universität Kassel, Mönchebergstraße 3, 34125 Kassel, Germany. ³Institut für Technische Chemie (Technical Chemistry), Universität Paderborn, Warburger Straße 100, 33098 Paderborn, Germany. ✉e-mail: wackenrohr@iw.uni-hannover.de

1

rates are still well below those of magnesium alloys, which can be in the range of up to 22.5 mm/year[16] (in 1% NaCl solution).

Another way for increasing the degradation is the use of constructive approaches, such as the integration of defined porosities or lattice structures, or the targeted application of defects stemming from AM processing. In particular, AM processes can be employed to specifically create open structures to promote crevice corrosion. In case of an AISI 316 L stainless steel processed by laser powder bed fusion (PBF-LB/M), it was possible to show that the corrosion behavior in general does not differ fundamentally from that of conventionally processed wrought alloys of the same type. However, the corrosion behavior changes as a result of the process-induced defects, which lead to a reduction in the re-passivation capability of the AM processed condition[17].

Besides the geometrical design advantages offered by AM, also other ways for alloy production and modification can be exploited, which cannot be realized in conventional processes, e.g., casting. For example, heterogeneous nucleation promoted by nano-scale particles can be exploited in the PBF-EB/M process after the addition of oxide particles, eventually significantly affecting the final microstructure established. This effect also has been demonstrated for a PBF-LB/M processed Al alloy in combination with ZrH_2 nanoparticles[18]. In addition to the grain refinement to be expected, as also shown for other alloys[18,19], the oxide particles themselves influence the conductivity within the powder bed in PBF-EB/M and, thus, the manufacturing process[20]. AM processing and various related aspects concerning material, synthesis and manufacturing of oxide dispersion strengthened alloys are detailed and discussed in Wilms et al. [21].

The material modifications presented in the present paper have already been investigated in a previous study with regard to the resulting microstructure and its evolution following AM[20]. In addition, the mechanical and the corrosive properties were investigated. The results can be summarized as follows:

The previous study investigated the effects of different amounts of Fe_2O_3 and CeO_2 nanoparticles on PBF-EB/M processed Fe. A significant refinement of the grain structure due to the use of oxides was not observed, as pure Fe is already characterized by relatively small grains due to the AM-specific intrinsic heat treatment and multiple phase transformations during layer-by-layer fabrication. Only the material with the lowest Fe_2O_3 content showed slightly smaller grain sizes compared to pure PBF-EB/M-Fe. Material modifications with CeO_2 were characterized by significant grain coarsening compared to pure PBF-EB/M-Fe. Only a slight decrease in grain sizes with increasing CeO_2 content was observed, which was attributed to the higher number of defects in this condition. The microstructural changes did not affect the texture. Differences seen in terms of grain sizes were primarily attributed to the different thermal histories of the material. Differences in prevailing temperatures were assumed to result from the different electrical resistivities and thermal conductivities of the powder modifications in the powder bed. The following conclusions can be drawn from the results[20]:

- The evolution of the microstructure is dominated by the prevailing temperature level during the PBF-EB/M process, in which always the same processing parameters were applied. The use of CeO_2 resulted in a strong coarsening of the microstructure, mainly due to the higher process temperatures. Refinement of the grain microstructure by oxides was hardly observed. The smallest grain sizes after PBF-EB/M processing were observed for pure Fe and for the Fe_2O_3 modification with the lowest fraction of nanoparticles.
- In the case of the Fe_2O_3 modifications, the resulting grain size clearly dominated the mechanical properties under quasistatic loading. In accordance to the Hall-Petch relationship, hardness, ultimate tensile strength, and yield strength increased with decreasing grain size.
- The mechanical properties showed more pronounced scatter in the case of CeO_2-modified conditions, which was due to the higher number of AM induced defects.

Pure PBF-EB/M manufactured Fe without any modification already has been examined regarding its corrosion-fatigue properties in Wackenrohr et al.[22]. The anticipated benefits of achieving a finer microstructure through PBF-EB/M processing, which could enhance fatigue life through the Hall Petch relation[23], were counterbalanced by defects introduced during the process, such as pores and lack of fusion. These defects further promoted the corrosion rates and, thus, the degradation.

As a continuation of the research in refs. 20 and 22, the modified materials initially processed by Torrent et al.[20] were investigated for their combined corrosion and fatigue properties in the present study. The objective here is to find a material condition with superior fatigue properties, which simultaneously fails earlier under the additional influence of corrosion. This condition is thought to be a perfect basis for a material with an increased degradation for the later use as degradable implant material.

Results

Corrosion-fatigue behavior of Fe_2O_3 modified PBF-EB/M-Fe

The results of the corrosion-fatigue tests in simulated body fluid (m-SBF) for the Fe_2O_3 modified conditions are shown in Fig. 1a–c in the form of S-N curves (stress amplitude $\Delta\sigma/2$ plotted over the number of cycles N). For better comparability, the results of pure PBF-EB/M-Fe from a previous study have been recompiled from Wackenrohr et al.[22]. For clarity, the test duration is also indicated on the x-axis.

For the condition with the lowest addition of Fe_2O_3 (Fig. 1a), the fatigue strength is slightly increased compared to the pure PBF-EB/M-Fe, especially in the high cycle fatigue (HCF) regime. One specimen reached the endurance limit (set as 5×10^6 Cycles) at 200 MPa, so the fatigue strength is increased by around 50 MPa compared to pure PBF-EB/M-Fe. For the tests under additional corrosive influence, the 0.011 wt.-% Fe_2O_3 modified condition also shows slightly increased fatigue strength and is, on average, about 50 MPa higher compared to the pure PBF-EB/M-Fe. An increase in the degradation, which would lead to an earlier failure and, eventually, to a steeper slope of the trendline, was not observed. The material state with a medium addition of oxides (0.022 wt.-% Fe_2O_3, Fig. 1b) generally shows an increased scatter in the fatigue life. In general, the fatigue strength decreases compared to the condition with the lowest addition of Fe_2O_3 (Fig. 1b), especially in the low cycle fatigue (LCF) range. Due to the more pronounced scatter, no clear conclusion can be drawn on the course of the individual trend lines for the 0.022 wt.-% Fe_2O_3 modified condition. For the condition with the highest addition of Fe_2O_3 (0.045 wt.-% Fe_2O_3, Fig. 1c), scatter increases again, so that the trend lines do not allow any clear comparison and interpretation, respectively. However, in general the fatigue strength decreases after adding higher amounts of oxides, i.e., more than 0.022 wt.-% of Fe_2O_3, compared to the pure PBF-EB/M-Fe.

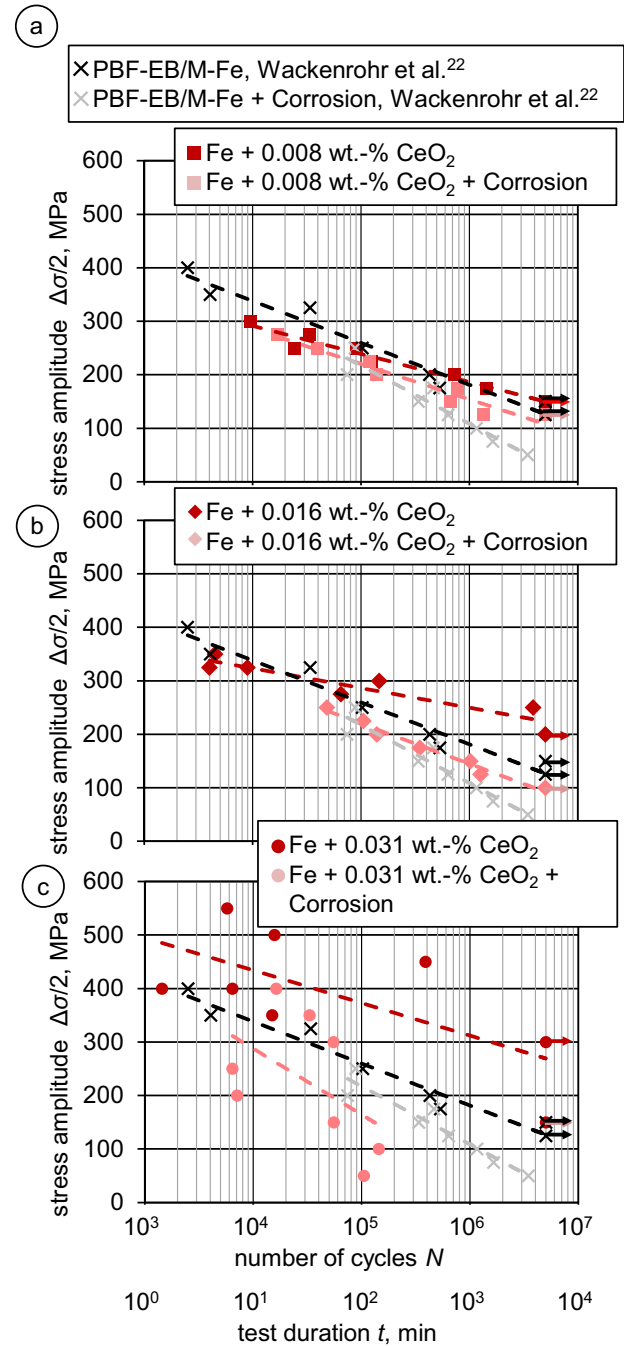### Corrosion-fatigue behavior of CeO_2 modified PBF-EB/M-Fe

The results of the corrosion-fatigue tests for the CeO_2 modified conditions are displayed in Fig. 2a-c. The material condition with the lowest addition of CeO_2 shows hardly any change in fatigue behavior compared to the PBF-EB/M-Fe (Fig. 2a). This holds true for the tests without and with additional corrosive influence. With increasing CeO_2 content (0.016 wt.-% CeO_2, Fig. 2b), the fatigue strength increases in the specimens tested without corrosive influence. The slope of the trendline decreases significantly in this case, compared to the pure PBF-EB/M-Fe. In addition, one specimen reached the endurance limit at 200 MPa. In the HCF regime the fatigue strength improved by about 50 MPa compared to the PBF-EB/M-Fe. Under additional corrosive influence, it can be seen that the fatigue behavior has hardly changed compared to the condition modified with 0.008 wt.-% CeO_2. An increase in the degradation, which would lead to a steeper slope of the trendline, was not observed for the conditions modified with 0.008 wt.-% CeO_2 and 0.016 wt.-% CeO_2. The largest impact on the fatigue properties can be seen for the condition with the highest fraction of CeO_2 (Fig. 2c). Without additional corrosive influence, the fatigue strength is significantly increased, as indicated by the lower slope of the trend line. The endurance
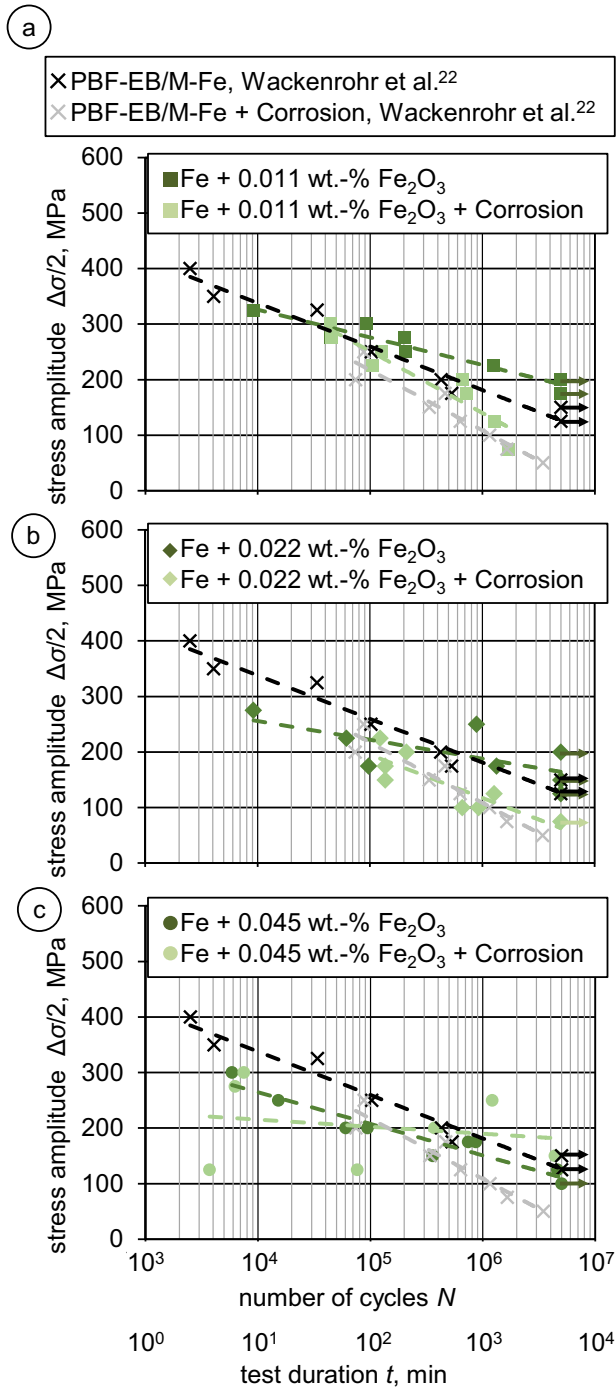
Fig. 1 | *S-N*-curves focusing on the Fe$_2$O$_3$ modified material states and pure PBF-EB/M-Fe. **a** Fe+ 0.011 wt.-% Fe$_2$O$_3$, **b** Fe+ 0.022 wt.-% Fe$_2$O$_3$, **c** Fe+ 0.045 wt.-% Fe$_2$O$_3$.

Fig. 2 | *S-N*-curves focusing on the CeO$_2$ modified material states and pure PBF-EB/M-Fe. **a** Fe+ 0.008 wt.-% CeO$_2$, **b** Fe+ 0.016 wt.-% CeO$_2$, **c** Fe+ 0.031 wt.-% CeO$_2$.

limit was found to be around 300 MPa, which was reached by one specimen. Compared to the PBF-EB/M-Fe the fatigue strength is about 100 MPa higher in the LCF range and 150 MPa higher in the HCF range. However, under additional corrosive influence there is a significant increase in the degradation. The specimens fail at distinctly lower number of cycles, so that no specimen reached the endurance limit. In general, the test results of the condition with the highest amount of CeO$_2$ are subject to more pronounced scatter compared to the conditions with a lower amount of oxides.

Fracture surfaces were examined by scanning electron microscopy (SEM). Figure 3 a depicts a representative fracture surface for Fe+ 0.031 wt.-% CeO$_2$ tested in air ($\Delta\sigma/2 = 350$ MPa, 1.5×10^4 cycles). On the fracture surface areas suffering lack of fusion (LoF) defects as well as less defective areas with fatigue-induced striations (Fig. 3b, c) can be seen. Figure 3d shows a specimen of Fe+ 0.031 wt.-% CeO$_2$ that was tested under the additional influence of corrosion ($\Delta\sigma/2 = 350$ MPa, 3.3×10^4 cycles). The formation of corrosion products on the fracture surface is clearly visible.

Discussion

Various influences of the particle modification on the manufacturing behavior and microstructure evolution have already been detailed and discussed in Torrent et al.[20]. Hence, the following discussion is limited to the corrosion-fatigue behavior of the modified conditions.

The approach to increase corrosion and degradation, respectively, for pure iron using powder modification before AM has already been

Fig. 3 | Representative images depicting fracture surfaces obtained by SEM (secondary electron contrast). a Fatigued Fe+ 0.031 wt.-% CeO_2 specimen tested in air ($\Delta\sigma/2 = 350$ MPa, 1.5×10^4 cycles) with an overview of the entire fracture area, areas with **b** LoF defects and **c** fatigue-induced striations. **d** Fatigued Fe+ 0.031 wt.-% CeO_2 specimen tested under mechanical load and corrosion ($\Delta\sigma/2 = 350$ MPa, 3.3×10^4 cycles).
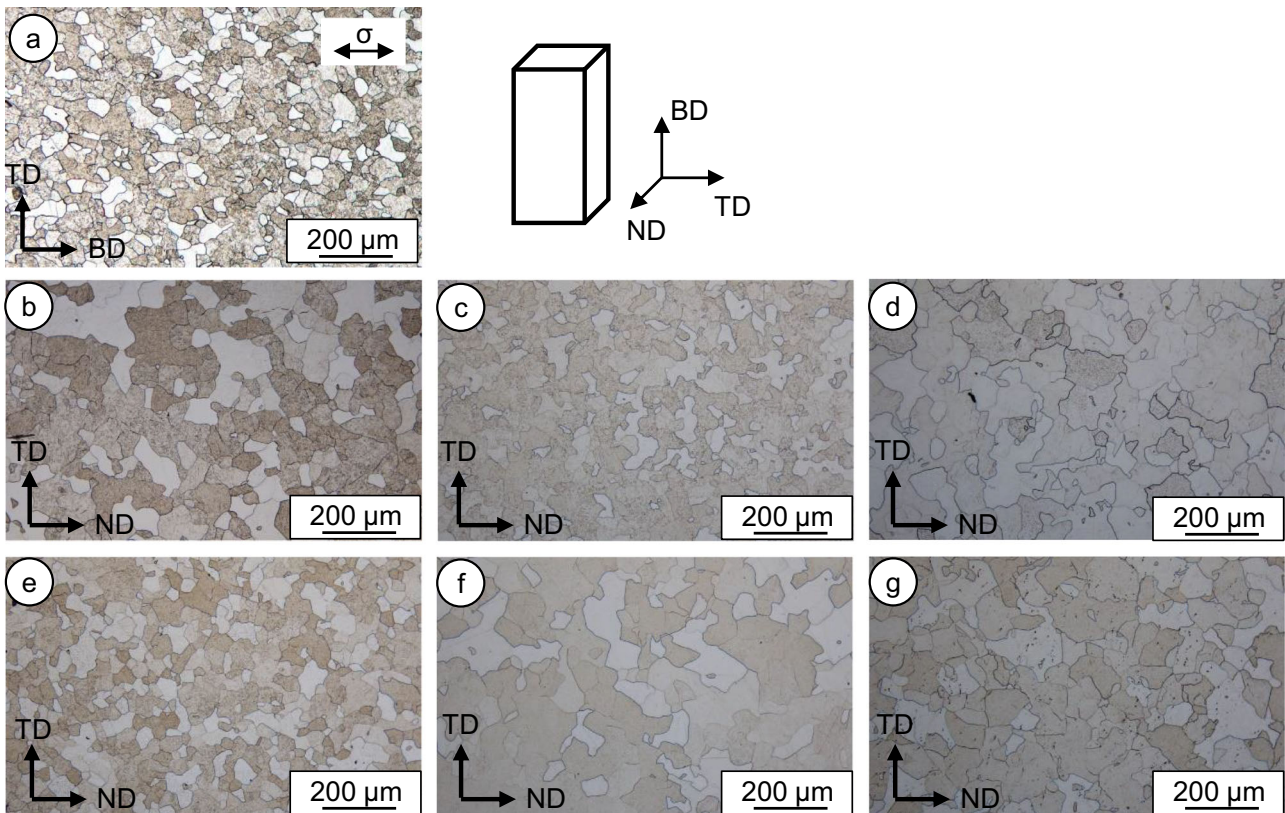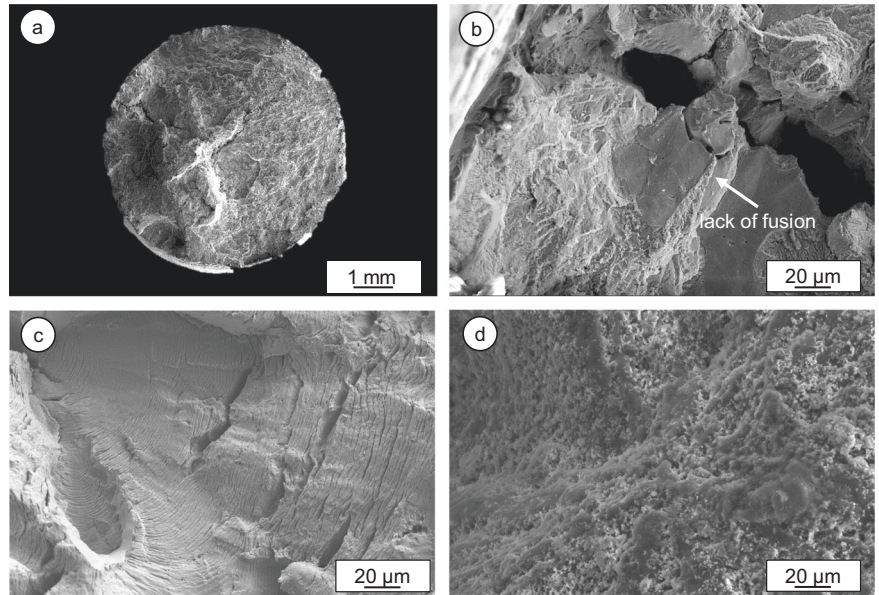
Fig. 4 | Micrographs of the material conditions in focus. All relevant directions are labeled. **a** Pure PBF-EB/M-Fe, **b** Fe+ 0.011 wt.-% Fe_2O_3, **c** Fe+ 0.022 wt.-% Fe_2O_3, **d** Fe+ 0.045 wt.-% Fe_2O_3, **e** Fe+ 0.008 wt.-% CeO_2, **f** Fe+ 0.016 wt.-% CeO_2, **g** Fe+ 0.031 wt.-% CeO_2.

successfully accomplished in various studies, e.g., by adding manganese and silver, respectively[24–26]. However, to the best of the authors' knowledge, in-depth studies on the corrosion-fatigue behavior of such alloys, as well as nanoparticle-modified alloys, are not yet available. In previous studies reporting on the corrosion-fatigue behavior of pure iron, it was shown that in case of PBF-EB/M processed conditions the degradation significantly increased compared to the conventionally processed condition, as indicated by a reduction in fatigue life under additional corrosive influence. The

increased degradation of the PBF-EB/M-Fe was attributed to the increased defect density following AM[22].

For the Fe_2O_3 modification, neither an increased density of process induced defects nor a change in texture could be detected in previous studies[20] (cf. Table 2). However, in the present study the fatigue strength is found to be inferior with increasing Fe_2O_3 content. This is in line with the results of the previous mechanical investigations (cf. Table 2). The mechanical properties showed decreasing tensile strengths and yield

strengths with increasing amounts of Fe_2O_3. The test results are therefore in good agreement with the Hall Petch relation[23]. It can accordingly be deduced that the changes in the mechanical properties can mainly be attributed to the altered properties during PBF-EB/M manufacturing, i.e., changes in thermal history due to variations in electrical resistivities and thermal conductivities of the powder bed. The Fe_2O_3 itself is thought not to cause any significant change in the microstructure in this case. The more pronounced scattering seen for the Fe_2O_3 modified conditions points at an inhomogeneous distribution of defects and pore sizes, respectively, which lead to inhomogeneous stress and strain distribution during fatigue testing. The impact of defects on fatigue properties and structural integrity of AM processed materials is subject of comprehensive research since years and has been summarized, e.g. in Zerbst et al.[27]. In the present study the Fe_2O_3 particles do not appear to have any further strengthening effect such as dispersion hardening, which would lead to increased fatigue strength at least for a number of specimens, where defects are not located in direct vicinity of the surface (i.e., for specimens located at the upper bound of the scatter band). Due to the even more pronounced scatter of results, no clear trends in the corrosion-fatigue properties can be observed. Still, in direct comparison to the tests conducted in air a decreased fatigue strength becomes obvious.

In contrast, the modification with CeO_2 shows promising results. With increasing content of CeO_2 the fatigue strength increases. At the same time the degradation increases, as can be seen from the different slopes of the trend lines within the S-N curves. The increase in degradation is also in good agreement with the increased corrosion rates reported in previous studies (see Table 2). In particular, the material condition with the highest CeO_2 content shows the highest initial corrosion rates (1.2×10^{-1} mm/year). These characteristics are of highest importance for the degradation behavior, especially under cyclic loading, since the protective oxide layer is repeatedly broken up at the crack tip. In addition, the oxide particles seem to form local galvanic elements that additionally promote degradation. Obviously, the condition with the highest amount of CeO_2 shows a more pronounced scattering compared to the pure PBF-EB/M-Fe. This is probably due to the increased defect density (cf. Fig. 4g). It was found in previous investigations that this modification is characterized by a more inhomogeneous defect distribution as well as pore size variations[20], eventually resulting in scattering of results under fatigue loading. It is expected that these defects also increase the degradation through their role as possible crack initiators and by promoting crevice corrosion. Still, the modification by CeO_2 seems to be characterized by an increased damage tolerance, so that the fatigue strength is not severely affected by those defects when tested without additional corrosive influence (cf. Fig. 2c). It is likely that localized effects stemming from dispersion strengthening play a role at this point, however, in situ studies focusing on initiation and growth of major defects under fatigue loading have to be conducted in future studies to clarify these effects. Clearly, the mechanical properties under quasistatic loading are not affected to the degree expected (cf. Table 2). The examination of the fracture surfaces for Fe+ 0.031 wt.-% CeO_2 revealed areas clearly suffering LoF as well as areas showing well-defined fatigue-induced striations (without any process-induced defects being present). No agglomerations of the CeO_2 nanoparticles were found on the fracture surface. This indicates a homogeneous distribution of the particles in the matrix, which further supports the rationale of dispersion strengthening. In summary, the role of CeO_2 with respect to the corrosion-fatigue behavior is not yet fully understood. Thus, the focus in future investigations is to further increase the amount of CeO_2 nanoparticles used for powder modification. A well-balanced composition is aimed for, i.e., a composition being characterized by simultaneous increase of fatigue strength as well as degradation, where both characteristics interact synergistically. These future studies, also exploiting the potentials of advanced in situ characterization techniques, will allow to achieve an in-depth understanding of the impacts of modification by CeO_2. Finally, the high damage tolerance of the CeO_2-modified states will be exploited to enable a specific adjustment of the porosity as an additional option to tailor the degradation properties of the implant material.

Methods

Powder modification and PBF-EB/M processing

Details on powder modification using Fe_2O_3 and CeO_2 and subsequent processing via PBF-EB/M are provided in Torrent et al.[20]. For processing an Arcam A2X PBF-EB/M machine (ARCAM AB, Mölndal, Sweden) was used, the process parameters are listed in Table 1.

Material properties (recompiled from Torrent et al.[20])

The material was investigated in detail in a previous study with regard to its microstructural properties, its mechanical characteristics and its electrochemical properties[20]. The main data from these investigations are summarized in Table 2. The corrosion rates were calculated on the basis of electrochemical impedance spectroscopy

Table 1 | Process parameters used for PBF-EB/M processing[20]

Strategy	Preheat	Melt
Meander, 90°	I = 15 mA	I = 12.25 mA
Hatch only	v = 12,000 mm/s	v = 4000 mm/s
Layer = 0.05 mm	12 repetitions	Hatch = 0.08 mm

Table 2 | Material properties of the different material modifications, recompiled from Torrent et al.[20]

	E-PBF-Fe	Fe+ 0.011 wt.-% Fe_2O_3	Fe+ 0.022 wt.-% Fe_2O_3	Fe+ 0.045 wt.-% Fe_2O_3	Fe+ 0.008 wt.-% CeO_2	Fe+ 0.016 wt.-% CeO_2	Fe+ 0.031 wt.-% CeO_2
Microstructural properties							
Average grain size in µm	27	23	29	48	67	66	54
Density in %	99.96	99.96	99.96	99.97	99.78	99.88	99.46
Mechanical properties							
Tensile yield strength (0.2%) in MPa	267	275	211	179	192	219	181
Ultimate yield strength in MPa	304	313	281	266	229	295	272
Total elongation in %	59.3	53.5	50.0	52.2	37.8	52.2	57.0
Hardness, HV 1	86	85.5	81	73	77	82.5	75.5
Electrochemical measured corrosion rates							
Corrosion rate in mm/year after 0 min	6.0×10^{-3}	2.2×10^{-2}	2.8×10^{-2}	2.7×10^{-3}	1.1×10^{-2}	3.9×10^{-2}	1.2×10^{-1}
Corrosion rate in mm/year after 1435 min	1.2×10^{-1}	5.3×10^{-2}	5.9×10^{-2}	7.2×10^{-2}	8.9×10^{-2}	6.3×10^{-2}	1.2×10^{-1}

Fig. 5 | Equipment for corrosion fatigue testing.
a Specimen geometry used for fatigue testing,
b schematic detailing the test setup applied for
corrosion fatigue testing.
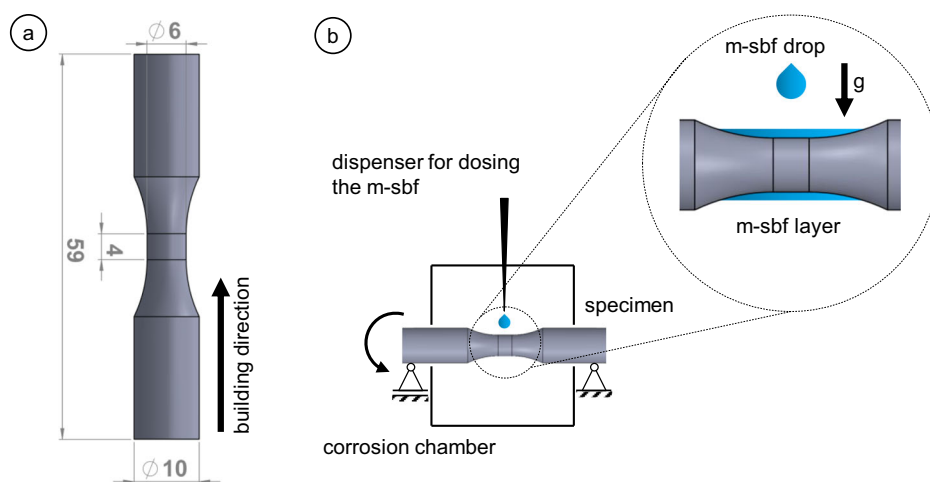
(EIS) data. The procedure and the analysis are described in Torrent et al.[20] in detail. It should be stated that a variation of the measured corrosion current density based on the surface state of the selected samples is not included in Table 2. The presented data should therefore be regarded as basis of discussion of the qualitative correlation between Fe_2O_3 and CeO_2 contents and the corrosion rate.

The microstructure for the different material conditions is shown in Fig. 4a–g. The grains that appear slightly darker result from the selective etching carried out using 2% alcoholic nitric acid. The building direction (BD), transversal direction (TD), normal direction (ND) and the loading direction (σ) are indicated in the figure. In addition to the different grain sizes (see Table 2), a slight increase in porosity can be seen for the state with the highest CeO_2 content (Fig. 4g). This could not be observed for the other material states (cf. also Table 2). Regardless of the degree of modification, all conditions are characterized by a ferritic microstructure.

Fatigue testing and specimen preparation

For the fatigue tests, rods with a diameter of 13 mm and a length of 59 mm were manufactured by PBF-EB/M. The final geometry was machined by turning and is shown in Fig. 5a, the building direction (BD) is labeled. Due to machining, no defects being related to the rough surface resulting from PBF-EB/M processing remained. All specimens were electrolytically polished. A surface roughness of $R_a \leq 0.1\ \mu m$ was obtained after polishing. The specimens were subjected to a rotating bending load at $1000\ min^{-1}$ on a Zwick Roell 200tC©. The endurance limit was set to 5×10^6 cycles. The stress amplitude ($\Delta\sigma/2$) was varied between 50 MPa and 550 MPa at a stress ratio of $R = -1$. For the additional corrosive influence, the specimens were constantly wetted with a m-SBF solution during the experiment. The composition of the m-SBF used is detailed in Oyane et al.[28]. The m-SBF solution was formulated to mimic the composition of blood plasma, with the exception of adjusting the concentration of HCO^{3-} to accommodate the presence of calcites. The solution constantly dripped from above onto the specimen at a flow rate of $150\ ml \times h^{-1}$. The rotation of the specimen promotes the formation of a constant liquid film on the specimen with a thickness of approx. 1 mm. The test setup is shown schematically in Fig. 5b. The temperature of the electrolyte was 25 °C. Based on the test frequency and the specified endurance limit, a maximum test duration of 83.3 h was set. For further details on the test setup readers are referred to previous studies[22,29].

Data availability

The data that support the findings of this study are available from the corresponding author upon request.

References

1. Frazier, W. E. Metal Additive Manufacturing: A Review. *J. Mater. Eng. Perform.* **23**, 1917–1928 (2014).
2. Murr, L. E. A Metallographic Review of 3D Printing/Additive Manufacturing of Metal and Alloy Products and Components. *Metallogr. Microstruct. Anal.* **7**, 103–132 (2018).
3. Hrabe, N., Gnäupel-Herold, T. & Quinn, T. Fatigue properties of a titanium alloy (Ti–6Al–4V) fabricated via electron beam melting (EBM): Effects of internal defects and residual stress. *Int. J. Fatigue* **94**, 202–210 (2017).
4. Romano, S. et al. Fatigue properties of AlSi10Mg obtained by additive manufacturing: Defect-based modelling and prediction of fatigue strength. *Eng. Fract. Mech.* **187**, 165–189 (2018).
5. Leuders, S. et al. On the mechanical behaviour of titanium alloy TiAl6V4 manufactured by selective laser melting: Fatigue resistance and crack growth performance. *Int. J. Fatigue* **48**, 300–307 (2013).
6. Torrent, C. J. J. et al. On the microstructural and cyclic mechanical properties of pure iron processed by electron beam melting. *Adv. Eng. Mater.* **327**, 2100018 (2021).
7. Li, Y. et al. In vitro degradation and biocompatibility evaluation of typical biodegradable metals (Mg/Zn/Fe) for the application of tracheobronchial stenosis. *Bioact. Mater.* **4**, 114–119 (2019).
8. Witte, F. The history of biodegradable magnesium implants: a review. *Acta Biomater.* **6**, 1680–1692 (2010).
9. Zheng, Y. F., Gu, X. N. & Witte, F. Biodegradable metals. *Mater. Sci. Eng. R* **77**, 1–34 (2014).
10. Niinomi, M., Nakai, M. & Hieda, J. Development of new metallic alloys for biomedical applications. *Acta Biomater.* **8**, 3888–3903 (2012).
11. Guo, Z. et al. Early effect of Ti–24Nb–4Zr–7.9Sn intramedullary nails on fractured bone. *Mater. Sci. Eng. C.* **29**, 963–968 (2009).
12. Peuster, M. et al. Long-term biocompatibility of a corrodible peripheral iron stent in the porcine descending aorta. *Biomater* **27**, 4955–4962 (2006).
13. Moravej, M., Prima, F., Fiset, M. & Mantovani, D. Electroformed iron as new biomaterial for degradable stents: development process and structure-properties relationship. *Acta Biomater.* **6**, 1726–1735 (2010).
14. Liu, B., Zheng, Y. F. & Ruan, L. In vitro investigation of Fe30Mn6Si shape memory alloy as potential biodegradable metallic material. *Mater. Lett.* **65**, 540–543 (2011).
15. Liu, B. & Zheng, Y. F. Effects of alloying elements (Mn, Co, Al, W, Sn, B, C and S) on biodegradability and in vitro biocompatibility of pure iron. *Acta Biomater.* **7**, 1407–1420 (2011).

16. Hort, N. et al. Magnesium alloys as implant materials-principles of property design for Mg-RE alloys. *Acta Biomater.* **6**, 1714–1725 (2010).

17. Kazemipour, M., Mohammadi, M., Mfoumou, E. & Nasiri, A. M. Microstructure and Corrosion Characteristics of Selective Laser-Melted 316L Stainless Steel: The Impact of Process-Induced Porosities. *JOM* **71**, 3230–3240 (2019).

18. Martin, J. H. et al. 3D printing of high-strength aluminium alloys. *Nature* **549**, 365–369 (2017).

19. Zhai, W., Zhu, Z., Zhou, W., Nai, S. M. L. & Wei, J. Selective laser melting of dispersed TiC particles strengthened 316L stainless steel. *Compos. B Eng.* **199**, 108291 (2020).

20. Torrent, C. J. J. et al. Oxide Modified Iron in Electron Beam Powder Bed Fusion—From Processability to Corrosion Properties. *Alloys* **1**, 31–53 (2022).

21. Wilms, M. B., Rittinghaus, S.-K., Goßling, M. & Gökce, B. Additive manufacturing of oxide-dispersion strengthened alloys: Materials, synthesis and manufacturing. *Prog. Mater. Sci.* **133**, 101049 (2023).

22. Wackenrohr, S. et al. Corrosion fatigue behavior of electron beam melted iron in simulated body fluid. *npj Mater. Degrad.* **6**, 18 (2022).

23. Hansen, N. Hall–Petch relation and boundary strengthening. *Scr. Mater.* **51**, 801–806 (2004).

24. Krüger, J. et al. Modification of Iron with Degradable Silver Phases Processed via Laser Beam Melting for Implants with Adapted Degradation Rate. *Adv. Eng. Mater.* **25**, 2201008 (2023).

25. Niendorf, T. et al. Processing of New Materials by Additive Manufacturing: Iron-Based Alloys Containing Silver for Biomedical Applications. *Metall. Mater. Trans. A* **46**, 2829–2833 (2015).

26. Wiesener, M. et al. Corrosion properties of bioresorbable FeMn-Ag alloys prepared by selective laser melting. *Mater. Corros.* **68**, 1028–1036 (2017).

27. Zerbst, U. et al. Damage tolerant design of additively manufactured metallic components subjected to cyclic loading: State of the art and challenges. *Prog. Mater. Sci.* **121**, 100786 (2021).

28. Oyane, A. et al. Preparation and assessment of revised simulated body fluids. *J. Biomed. Mater. Res. Part A* **65**, 188–195 (2003).

29. Huang, J. et al. Influence of hydrogel coatings on corrosion and fatigue of iron in simulated body fluid. *Mater. Corros.* **73**, 1034–1044 (2022).

Author contributions

S.W. was responsible for fatigue life investigation and writing of the paper. C.J.J.T. and J.-M.F. were responsible for additive manufacturing. C.E. and M.V. did the powder modification. S.H. and P.K. helped to interpret the experimental data. G.G., T.N., F.N. and H.J.M.: conceptualization, review and supervision of the study.

Competing interests

The authors declare no competing interests.

Additional information

Correspondence and requests for materials should be addressed to Steffen Wackenrohr.

Reprints and permissions information is available at http://www.nature.com/reprints

Publisher's note Springer Nature remains neutral with regard to jurisdictional claims in published maps and institutional affiliations.